Supplement of The Cryosphere, 15, 17–30, 2021
https://doi.org/10.5194/tc-15-17-2021-supplement

The Cryosphere
Open Access

Supplement of

Subglacial carbonate deposits as a potential proxy for a glacier's former presence

Matej Lipar et al.

Correspondence to: Matej Lipar (matej.lipar@zrc-sazu.si)

Supplementary Figure S1: Photographic material of the retreating Triglav Glacier (© ZRC SAZU Anton Melik Geographical Institute archive).

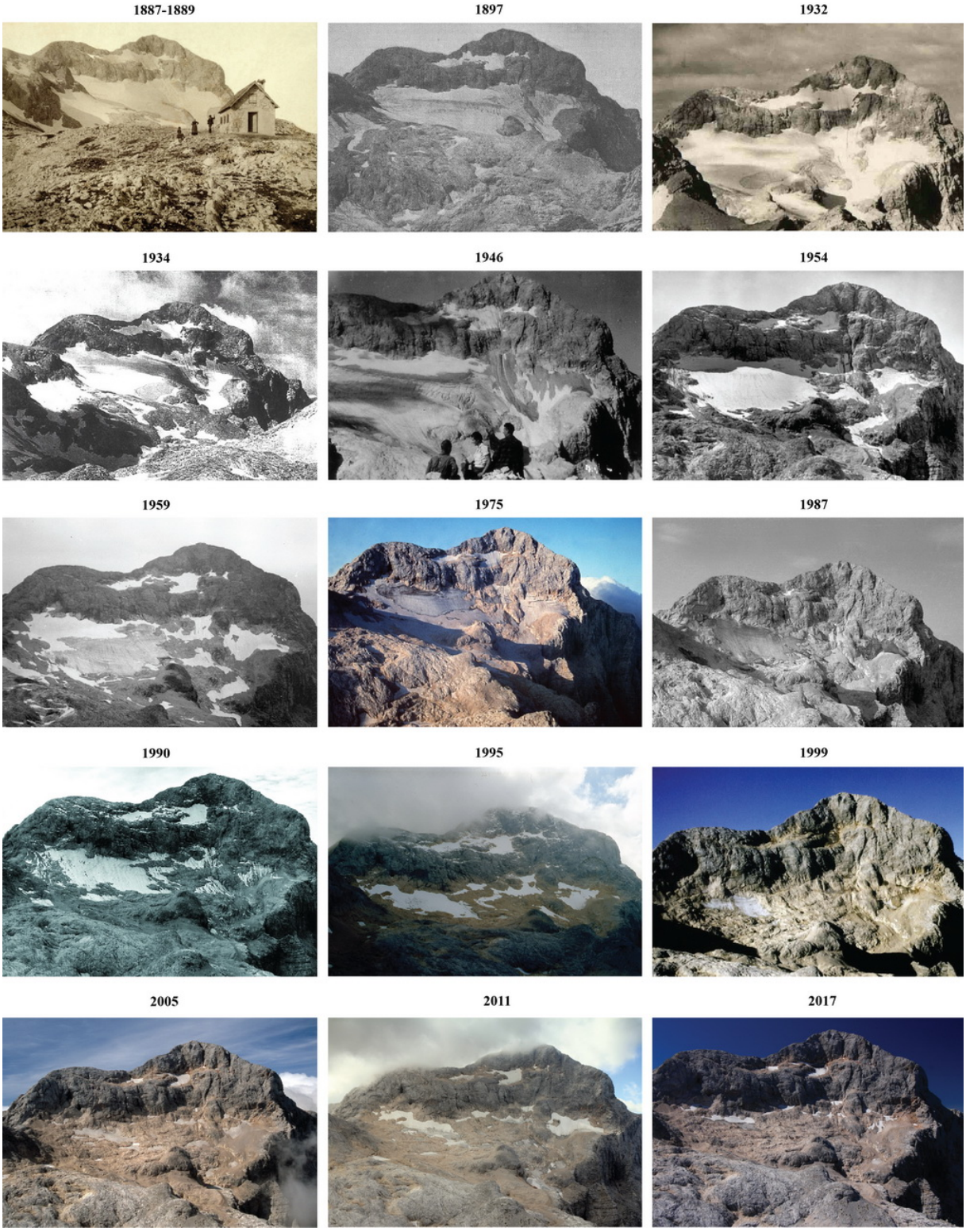

Supplementary Figure S2: Locality aerial map of the Triglav Glacier, the sampling sites discussed in the text, and general geomorphology.

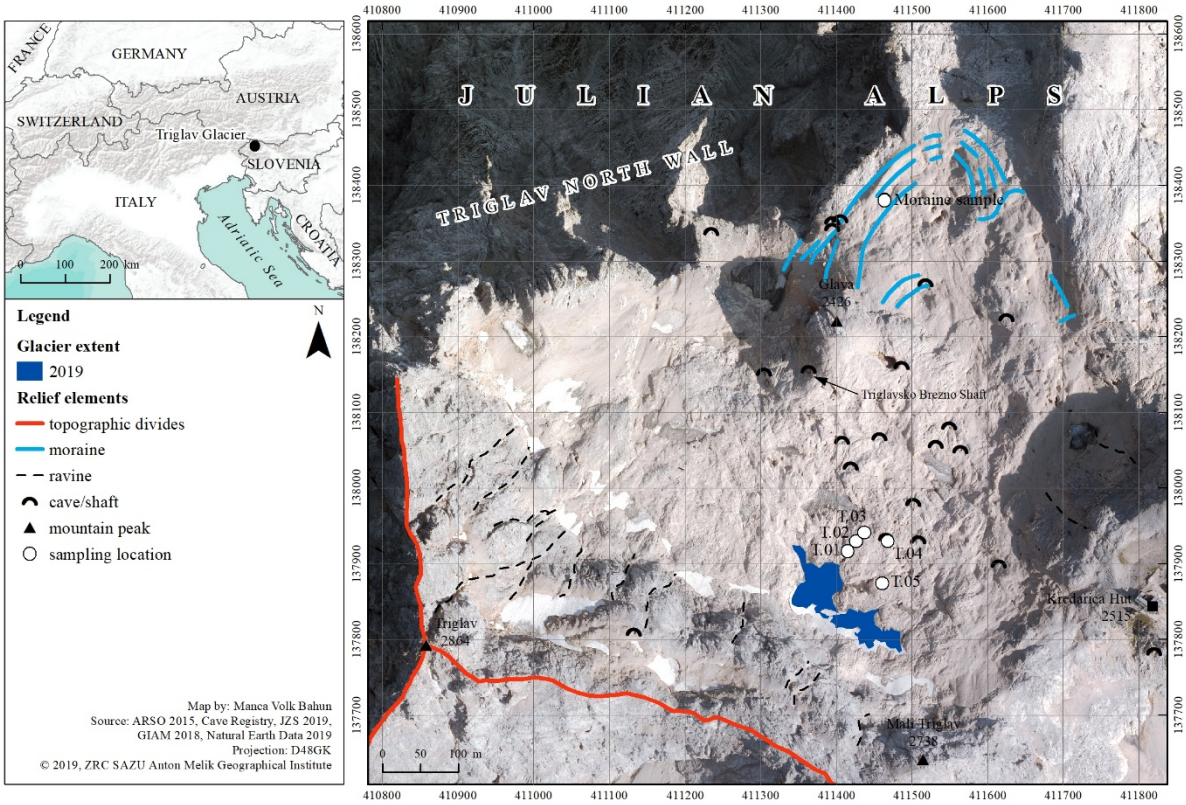

Supplementary Figure S3: Average ablation season temperature (May – October) on meteorological station Kredarica (Fig. 1) between 1955 and 2018. Data source: Slovenian Environment Agency.

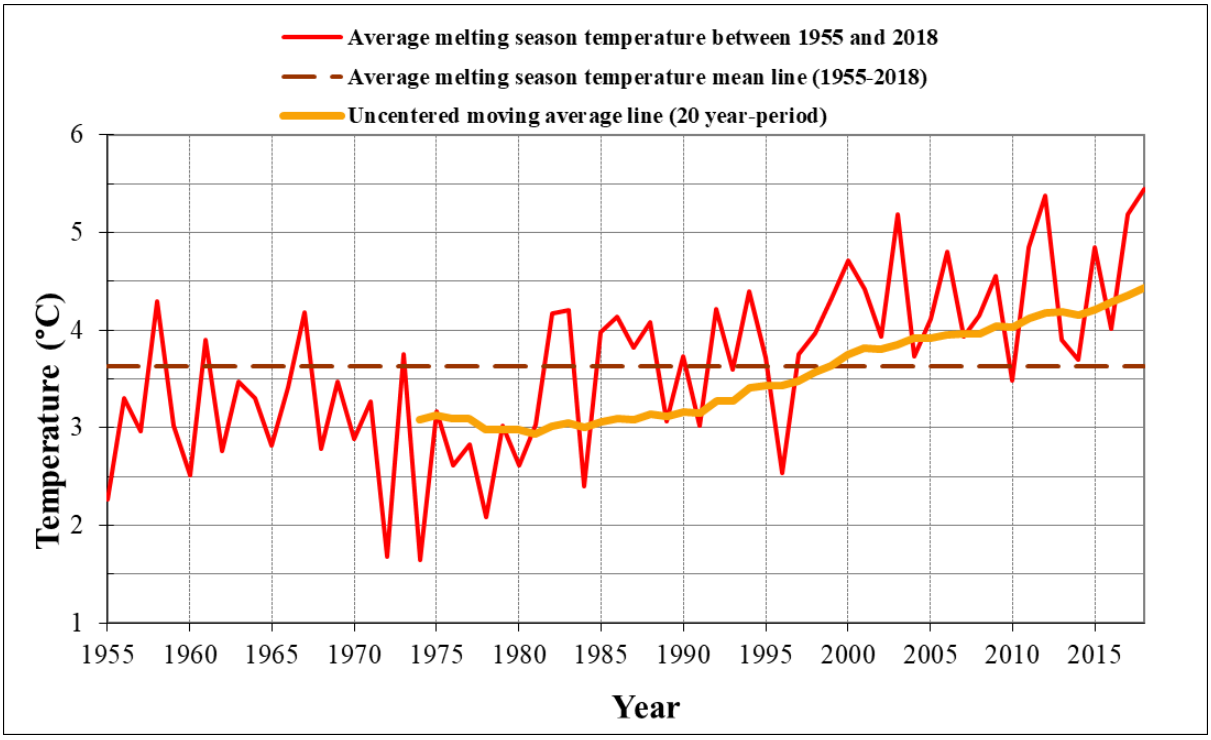

Supplementary Figure S4: Reconstruction of the highest seasonal snow height on the edge of the Triglav Glacier between 1852 and 2018 updated from Gabrovec et al. (2014) (source: Slovenian Environment Agency (from 1955 on), reconstruction/reanalysis before 1955 done by Jaka Ortar).

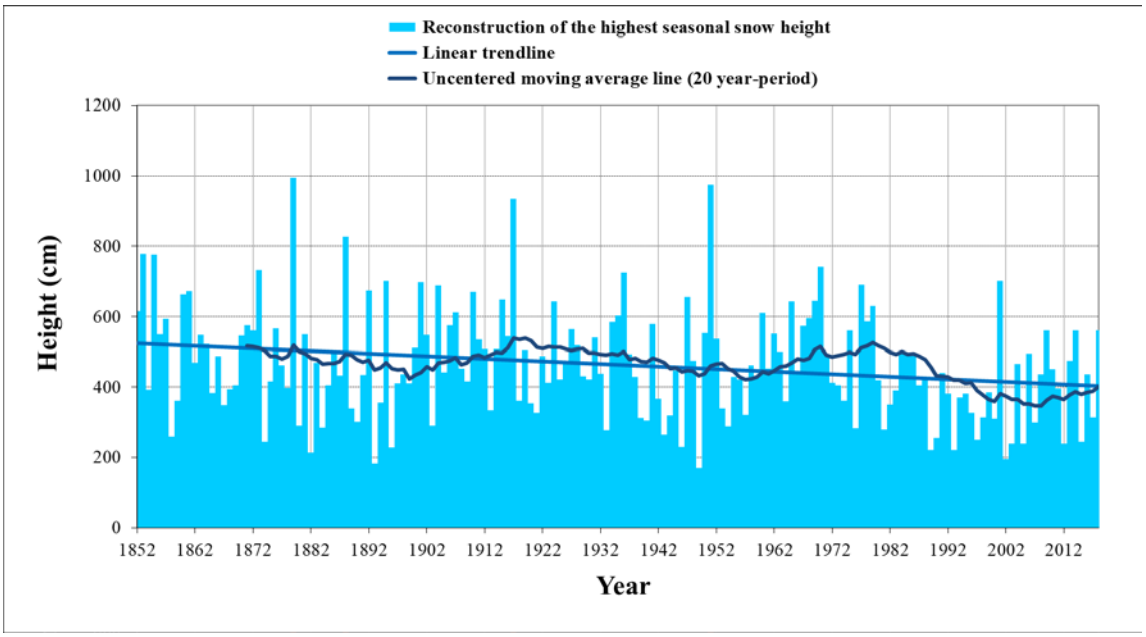

Supplementary Figure S5: XRD diagrams of all the studied samples (for precise location, see Figure 3 in the main manuscript). Samples TRG-01 C and TRG-03 D correspond to the bed rock. Green lines mark the reflections corresponding to calcite, and red lines mark the reflections of those corresponding to aragonite.

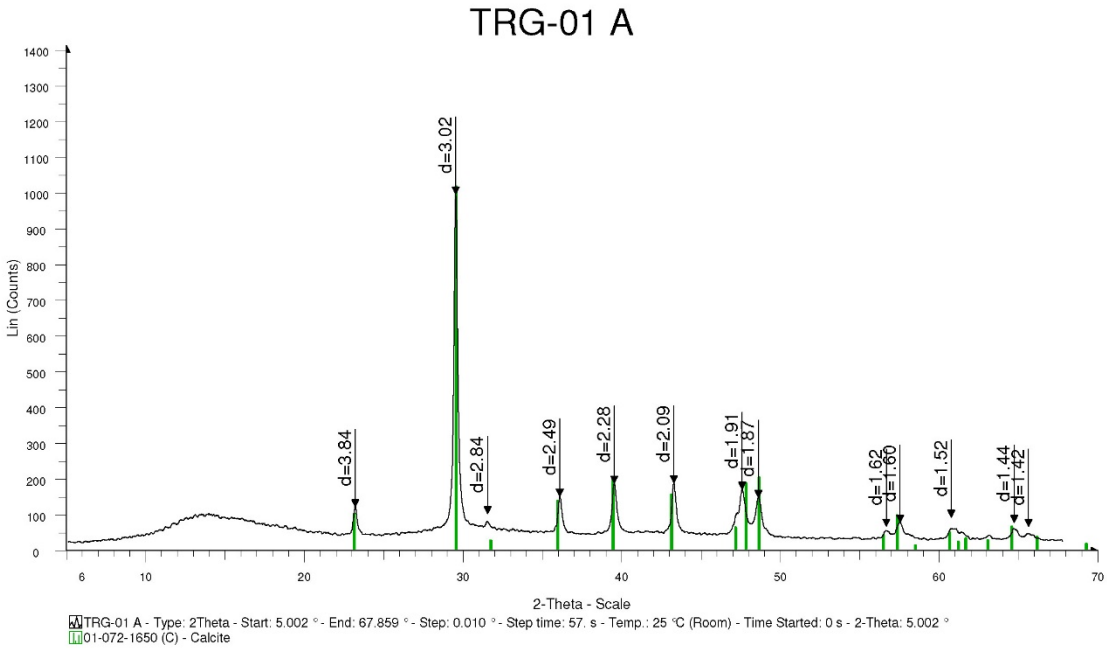

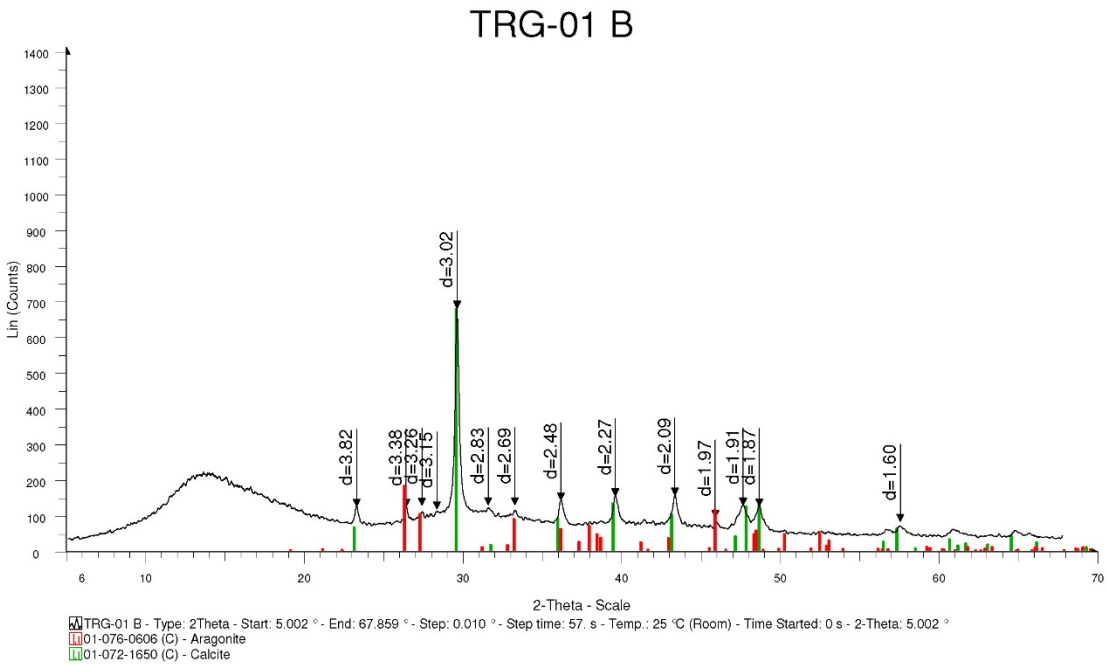

TRG-01 C

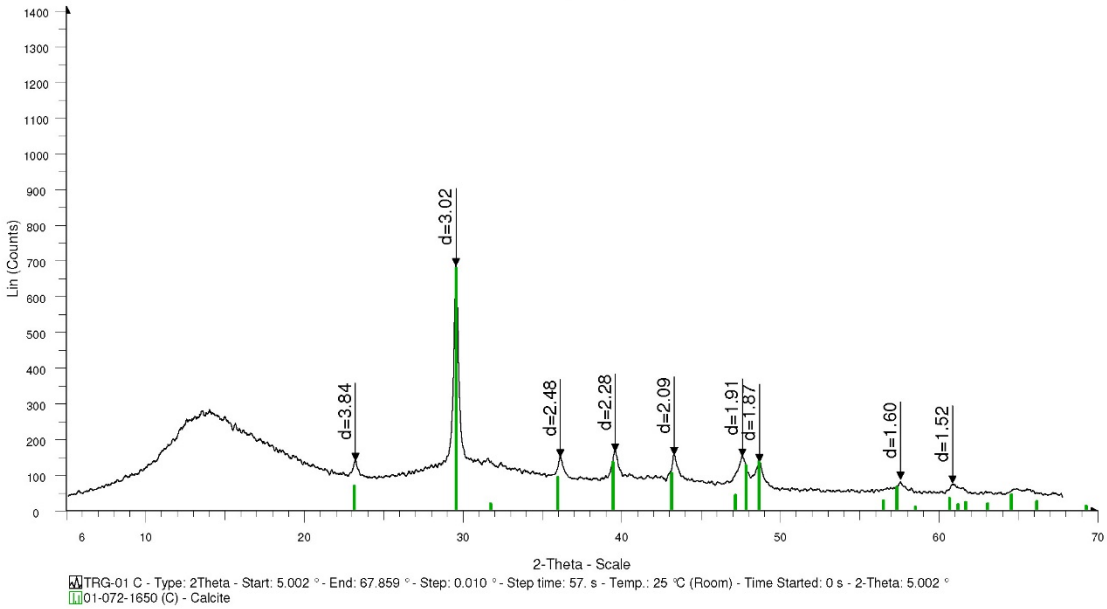

TRG-02

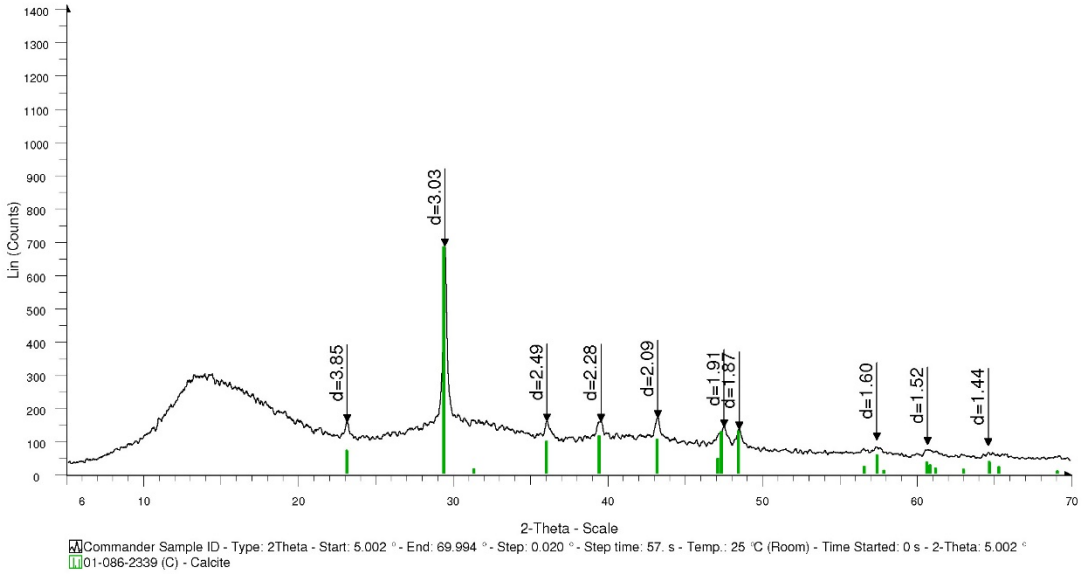

TRG-03 A

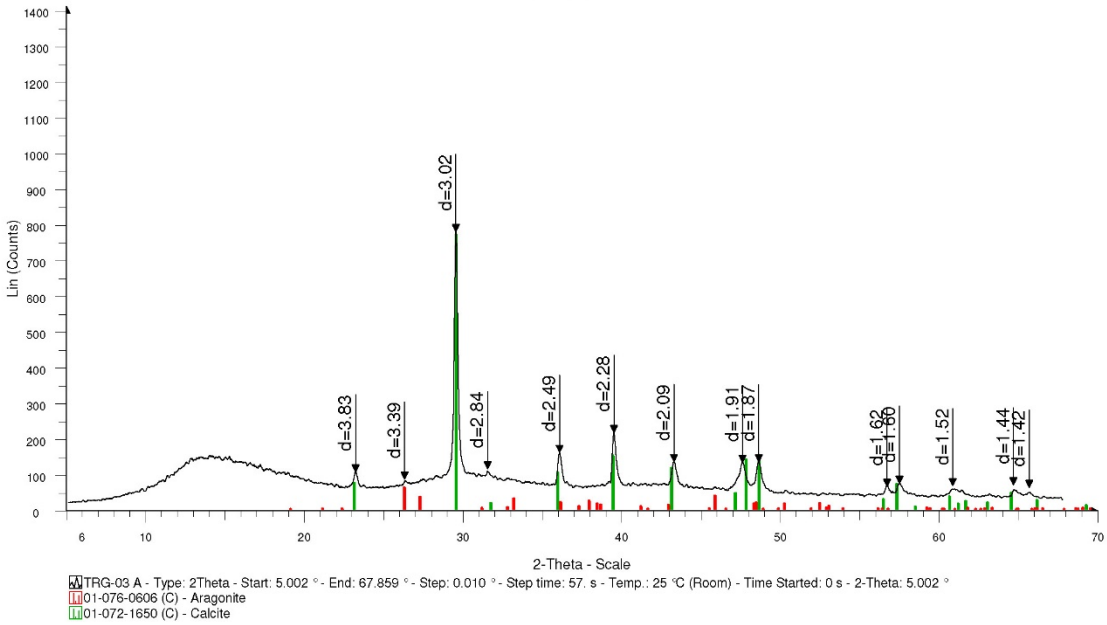

TRG-03 B

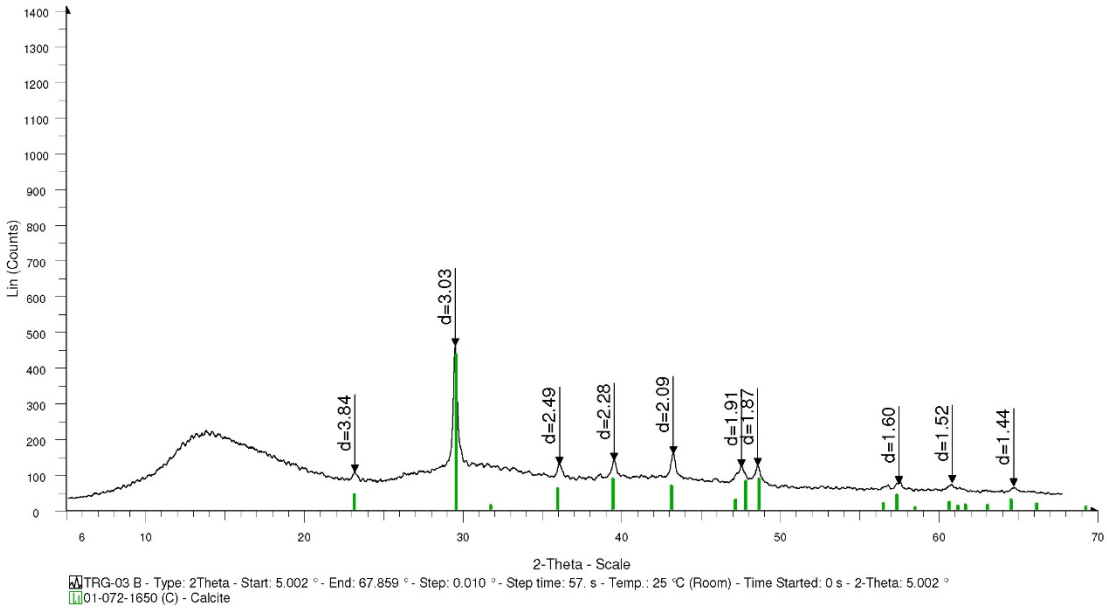

TRG-03 C

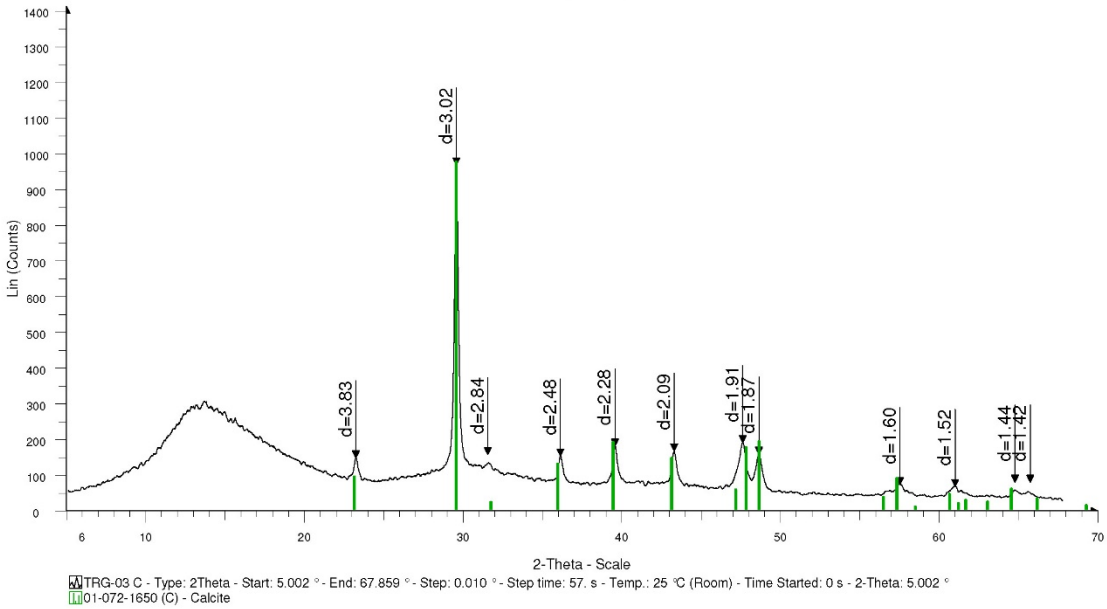

TRG-03 D

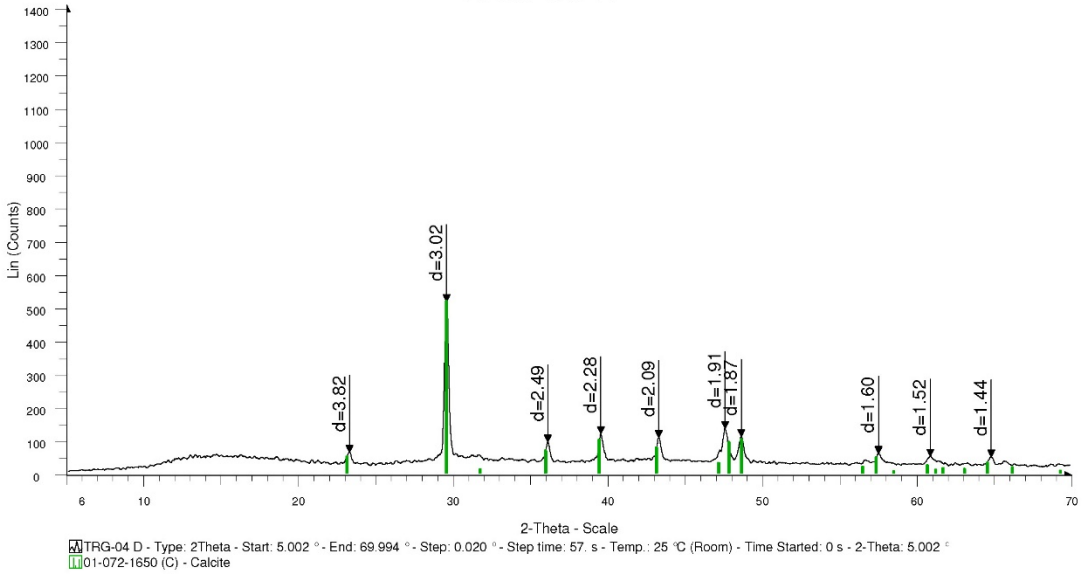

TRG-04 A

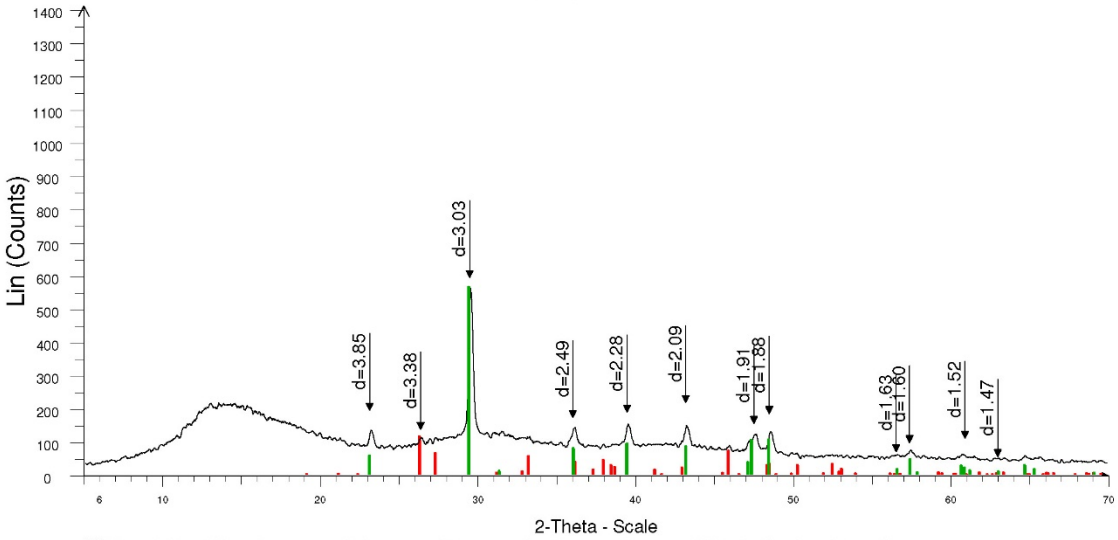

TRG-04 A - Type: 2Theta - Start: 5.002 ° - End: 69.994 ° - Step: 0.020 ° - Step time: 57. s - Temp.: 25 °C (Room) - Time Started: 0 s - 2-Theta: 5.002 °
01-086-2339 (C) - Calcite
01-076-0606 (C) - Aragonite

TRG-04 B

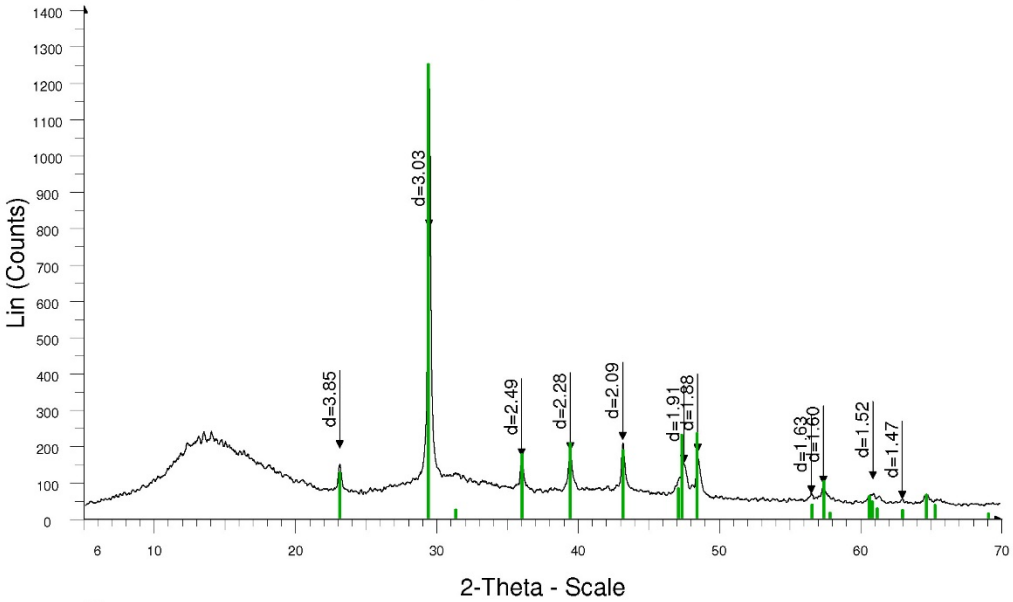

TRG-04 B - Type: 2Theta - Start: 5.002 ° - End: 69.994 ° - Step: 0.020 ° - Step time: 57. s - Temp.: 25 °C (Room) - Time Started: 0 s - 2-Theta: 5.002 °
Operations: Smooth 0.150 | Import
01-086-2339 (C) - Calcite

TRG-04 C

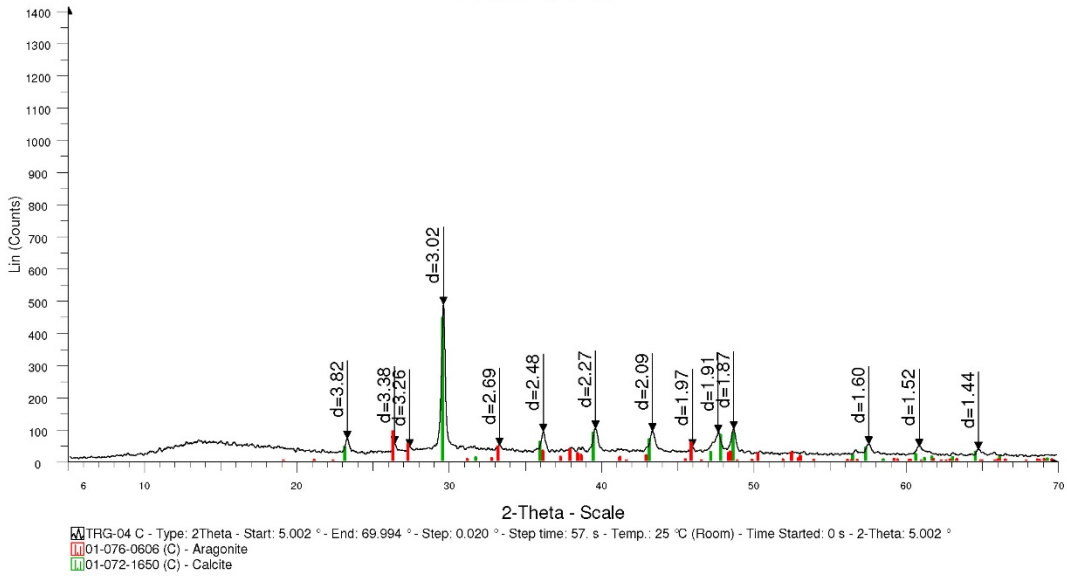

TRG-05

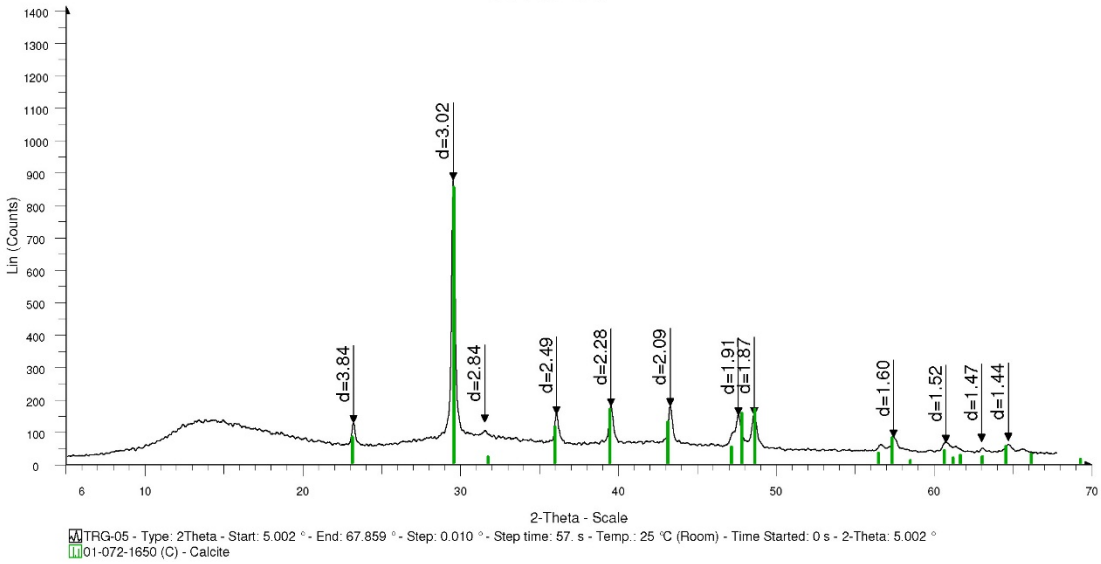

Supplementary Figure S6: a) Short columnar calcite crystals alternating with brown micritic bands constitute the first calcite precipitates over the host rock. Plane polarised light (PPL); b) columnar calcite crystals predominantly oriented towards the right (downslope). Crossed polarised light (XPL); c) oriented columnar calcite crystals displaying signs of dissolution. Occasionally, both crystal layers are separated by a thin, wavy micritic layer possibly indicating dissolution processes (PPL); d) aragonite-calcite layered textures (right) and secondary calcite crystals with aragonite relicts, some of them arranged in fans aligned forming a band (PPL); e) secondary calcite showing abundant aragonite relicts and very anhedral textures (PPL); f) the same image as e, under crossed polarised light. Thin sections orientation is parallel to the former glacier sliding direction.

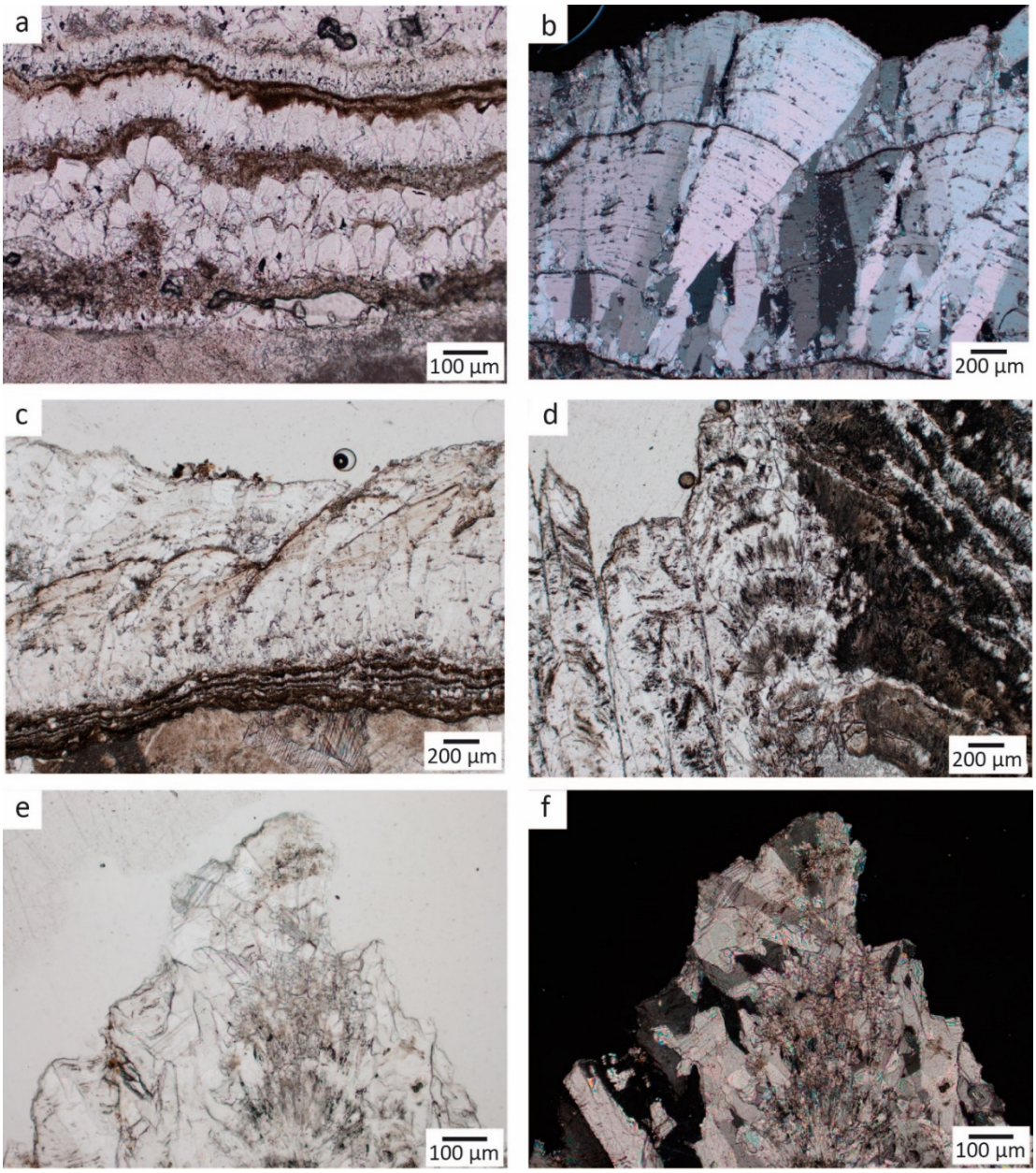

Supplementary Figure S7: The columnar and elongated columnar calcite crystals oriented downslope (plane polarised light – above, and crossed polarised light – below). Thin section orientation is parallel to the former glacier sliding direction.

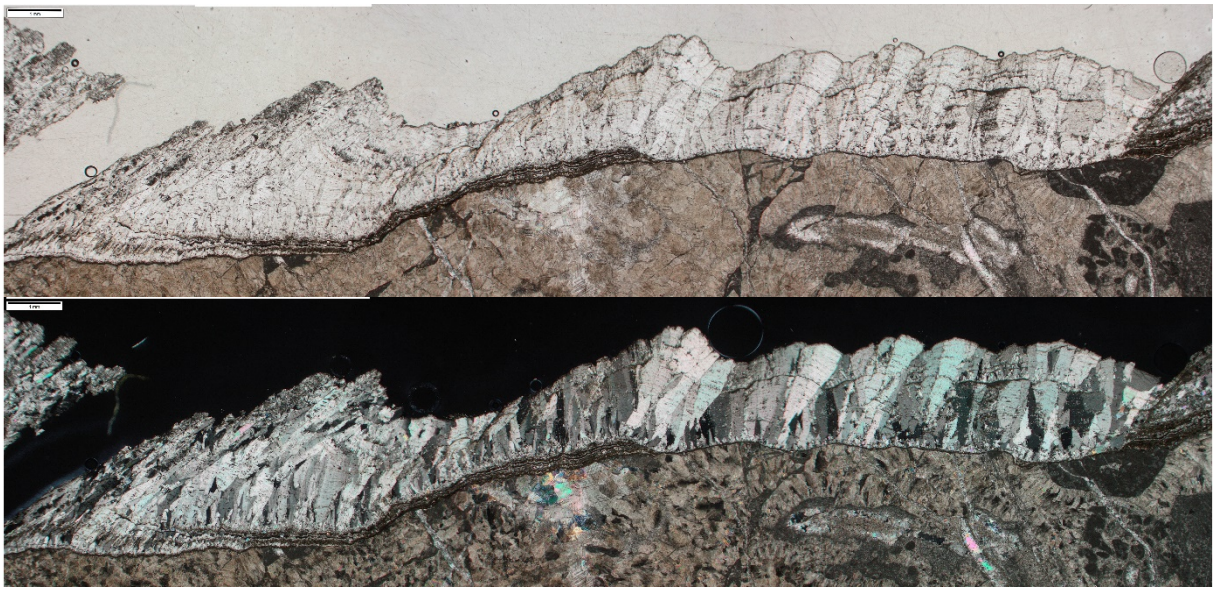

Supplementary Table S1: U-Th data for the subglacial calcite. Note: Ratios in parentheses are activity ratios calculated from the atomic ratios. Errors are at 2δ level. The ages are calculated using the Isoplot 3.75 Program of Ludwig (2012) with decay constants from Cheng et al. (2000). Corrected Ages were calculated assuming initial/detrital $^{230}Th/^{232}Th$ activity ratio equal 0.825 ± 50 % (the bulk-Earth value, which is the most commonly used for initial/detrital ^{230}Th corrections).

U-Th dating was carried out using a Nu Plasma multi-collector inductively-coupled plasma mass spectrometer (MC-ICP-MS) in the Radiogenic Isotope Facility (RIF) at the School of Earth and Environmental Sciences, The University of Queensland (UQ) following chemical treatment procedures and MC-ICP-MS analytical protocols described elsewhere (Zhao et al., 2009; Clark et al., 2012; Clark et al., 2014). Powdered or chipped sub-samples weighing 16–78 mg were spiked with a mixed ^{229}Th-^{233}U tracer and then completely dissolved in concentrated HNO_3. After digestion, each sample was treated with H_2O_2 to decompose trace amounts of organic matters (if any) and to facilitate complete sample-tracer homogenisation. U and Th were separated using conventional anion-exchange column chemistry using Bio-Rad AG 1-X8 resin. After stripping off the matrix from the column using double-distilled 7N HNO as eluent, 3 ml of a 2% HNO_3 solution mixed with trace amount of HF was used to elute both U and Th into a 3.5-ml pre-cleaned test tube, ready for MC-ICP-MS analyses, without the need for further drying down and re-mixing. After column chemistry, the U-Th mixed solution was injected into the MC-ICP-MS through a DSN-100 desolvation nebuliser system with an uptake rate of around 0.07 ml per minute. U-Th isotopic ratio measurement was performed on the MC-ICP-MS using a detector configuration to allow simultaneous measurements of both U and Th isotopes (Zhou et al., 2011; Clark et al., 2014). The $^{230}Th/^{238}U$ and $^{234}U/^{238}U$ activity ratios of the samples were calculated using the decay constants given in (Cheng et al., 2000). The non-radiogenic ^{230}Th was corrected using an assumed bulk-Earth atomic $^{230}Th/^{232}Th$ ratio of $4.4 \pm 2.2 \times 10^{-6}$. U-Th ages were calculated using the Isoplot/Ex 3.75 Program (Ludwig, 2012).

Sample Name	**Sample wt.(g)**	**U (ppm)**	**±2s**	**^{232}Th (ppb)**	**±2s**	**($^{230}Th/^{232}Th$)**	**±2s**	**($^{230}Th/^{238}U$)**	**±2s**	**($^{234}U/^{238}U$)**	**±2s**	**uncorr. ^{230}Th Age (ka)**	**±2s**	**corr. ^{230}Th Age (ka)**	**±2s**	**corr. Initial ($^{234}U/^{238}U$)**	**±2s**
T.01_a1	0,06022	0,45584	0,00019	20,522	0,019	10,945	0,047	0,1624	0,0007	0,9787	0,0012	19,83	0,10	**18,45**	**0,70**	0,9773	0,0013
T.03_a1	0,07823	0,41066	0,00017	7,454	0,012	19,219	0,103	0,1150	0,0006	1,0053	0,0005	13,26	0,07	**12,72**	**0,28**	1,0055	0,0006
T.03_a2	0,02380	0,8933	0,0003	4,929	0,005	19,99	0,23	0,0363	0,0004	1,0062	0,0011	4,012	0,047	**3,849**	**0,094**	1,0063	0,0011
T.03_b1	0,01620	1,7737	0,0005	4,080	0,005	24,49	0,23	0,0186	0,0002	1,0079	0,0008	2,027	0,019	**1,959**	**0,039**	1,0079	0,0008
T.05	0,02151	1,3305	0,0004	68,59	0,11	12,20	0,05	0,2072	0,0008	1,0060	0,0010	25,15	0,11	**23,62**	**0,78**	1,0065	0,0011

References:

Cheng, H., Edwards, R. L., Hoff, J., Gallup, C. D., Richards, D. A., and Asmerom, Y.: The half-lives of uranium-234 and thorium-230, Chemical Geology, 169, 17-33, doi:10.1016/s0009-2541(99)00157-6, 2000.

Clark, T. R., Zhao, J.-x., Feng, Y.-x., Done, T. J., Jupiter, S., Lough, J., and Pandolfi, J. M.: Spatial variability of initial $^{230}Th/^{232}Th$ in modern Porites from the inshore region of the Great Barrier Reef, Geochimica et Cosmochimica Acta, 78, 99-118, doi:10.1016/j.gca.2011.11.032, 2012.

Clark, T. R., Zhao, J.-X., Roff, G., Feng, Y.-X., Done, T. J., Nothdurft, L. D., and Pandolfi, J. M.: Discerning the timing and cause of historical mortality events in modern Porites from the Great Barrier Reef, Geochimica et Cosmochimica Acta, 138, 57-80, doi:10.1016/j.gca.2014.04.022, 2014.

Gabrovec, M., Hrvatin, M., Komac, B., Ortar, J., Pavšek, M., Topole, M., Triglav Čekada, M., and Zorn, M.: Triglavski ledenik [Triglav Glacier], Založba ZRC, Ljubljana, 2014.

Ludwig, K. R.: User's manual for Isoplot version 3.75–4.15: a geochronological toolkit for Microsoft Excel, Berkeley Geochronological Center Special Publication, 5, 2012.

Zhao, J.-x., Yu, K.-f., and Feng, Y.-x.: High-precision ^{238}U–^{234}U–^{230}Th disequilibrium dating of the recent past: a review, Quaternary Geochronology, 4, 423-433, doi:10.1016/j.quageo.2009.01.012, 2009.

Zhou, H., Zhao, J., Qing, W., Feng, Y., and Tang, J.: Speleothem-derived Asian summer monsoon variations in Central China, 54-46 ka, Journal of Quaternary Science, 26, 781-790, doi:10.1002/jqs.1506, 2011.